Mechanics of Advanced Materials and Structures

ISSN: (Print) (Online) Journal homepage: https://www.tandfonline.com/loi/umcm20

Free vibration by length-scale separation and inertia-induced interaction –application to large thin-walled structures

Aleksi Laakso, Jani Romanoff, Ari Niemelä, Heikki Remes & Eero Avi

To cite this article: Aleksi Laakso, Jani Romanoff, Ari Niemelä, Heikki Remes & Eero Avi (2022): Free vibration by length-scale separation and inertia-induced interaction –application to large thin-walled structures, Mechanics of Advanced Materials and Structures, DOI: 10.1080/15376494.2022.2029981

To link to this article: https://doi.org/10.1080/15376494.2022.2029981

Published online: 14 Feb 2022.

MECHANICS OF ADVANCED MATERIALS AND STRUCTURES
https://doi.org/10.1080/15376494.2022.2029981

Taylor & Francis
Taylor & Francis Group

ORIGINAL ARTICLE

Free vibration by length-scale separation and inertia-induced interaction –application to large thin-walled structures

Aleksi Laakso[a,b], Jani Romanoff[a], Ari Niemelä[b], Heikki Remes[a], and Eero Avi[a]

[a]Department of Mechanical Engineering, Aalto University School of Engineering, Espoo, Finland; [b]Structural Design, Meyer Turku Oy, Turku, Finland

ABSTRACT

This paper analyses free vibration of interacting length-scales of 3D-thin-walled structures by combination of Finite Elements Method and analytical calculation of strain and kinetic energies. Equivalent single layer elements with structurally homogenized mass and stiffness enable significantly reduced computational cost. Analytical equations are used to re-introduce effects of inertia-induced deformations of the local length-scale that are restrained by the kinematic of homogenized equivalent single layer elements. The method is validated against fine mesh Finite Element Analysis in a case study representing typical 3D-structure seen in cruise ships. The method achieves excellent accuracy for the 10 first natural modes.

ARTICLE HISTORY
Received 16 September 2021
Accepted 11 January 2022

KEYWORDS
Free vibration; length-scale interaction; finite element method; energy method; thin-walled structure; ship structure

Nomenclature

A	generalized amplitude
B	normalization factor
c	response coefficient
D	plate bending stiffness
$\boldsymbol{e}$	orientation vector
E	mechanical energy/Young's modulus
f	natural frequency (Hz)
F	reaction force
H	set of structures not included in P
$\boldsymbol{i}, \boldsymbol{j}, \boldsymbol{k}$	global base vectors
K	generalized stiffness
K	stiffness matrix (FEM)
L	length/primary stiffener spacing
m	mass per unit area
M	generalized mass/Reaction moment in Figure 4
M	mass matrix (FEM)
N	total number of stiffened panels in R
P	set including plates in way of stiffened panels
r	response
R	set including the whole structure
s	local coordinate (distance from stiffener)
S	stiffener spacing (secondary stiffeners)
t	time/thickness
T	kinetic energy
U	strain energy (spring potential energy)
w	displacement
X, Y, Z	global coordinates

Greek symbols

α	area
β	dimensionless natural frequency parameter
λ	local wavelength
ν	Poisson's ratio
ξ	generalized coordinate
ρ	material mass density
σ	dimensionless natural frequency parameter
Ψ	mode shape (displacement)
ω	natural frequency (rad/s)

Subscripts and superscripts

d	dynamic
G	global
i	iteration step number
L	local
m	mode number
n	node (FEM) number
NS	nonstructural
p	stiffened panel number
peak	peak value
R	relative
s	static
x	stiffened plate direction of secondary stiffeners
y	stiffened plate in plane direction perpendicular to x
z	stiffened plate normal direction

1. Introduction

Free vibration is one of the most fundamental natural phenomena studied by the classical mechanics. In the 19thcentury, Lord Rayleigh presented well-known overview of the physics of mechanical vibrations [1]. By starting from kinetic and strain energies, Rayleigh derived exact equations of motion for continuous systems with simple kinematic assumptions such as strings, bars and plates. Additionally, he considered

CONTACT Aleksi Laakso aleksi.laakso@aalto.fi Department of Mechanical Engineering, Aalto University School of Engineering, Espoo, Finland.

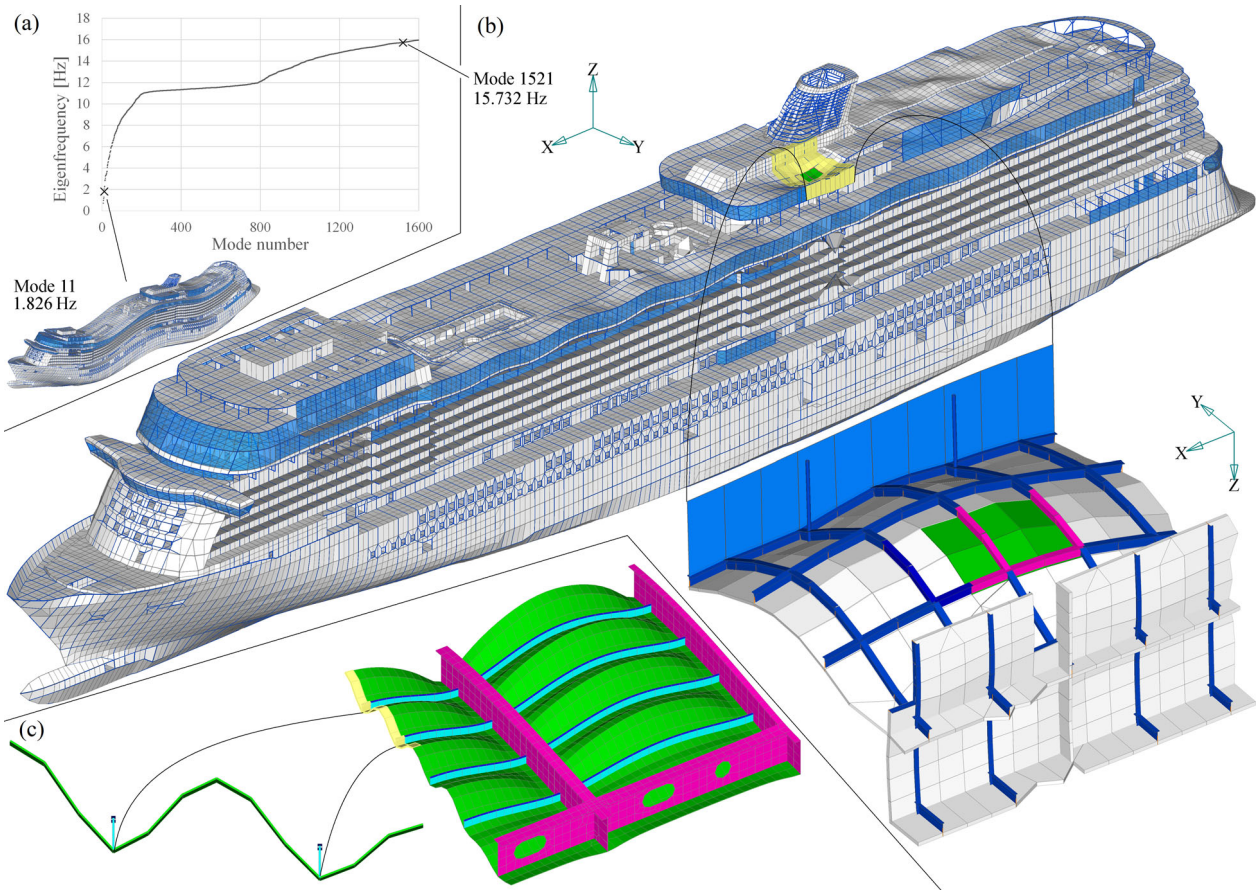

Figure 1. (a) Frequency range of modes of a typical cruise ship structure. (b) Example of a mode in a frequency range where wide range of length-scales are deforming simultaneously, obtained by FEM model with plates and secondary stiffeners modeled by ESL. (c) Sketch of secondary stiffener and plate deformations if fine shell element mesh was used.

free vibration of 'approximately simple systems' by utilizing mode shapes of a simple system (e.g. string with uniform density) to analyze slightly altered system (string with slightly non-uniform density). He recalculated the kinetic and strain energies by applying mode shapes of the simple system and system parameters (density) of the altered system to find approximate solutions for the latter. This paper applies similar logic in the context of the Finite Element Method (FEM) and 3D thin-walled structures.

Advances in solid mechanics and mathematics through the 20th century along with emerge of the digital computers eventually lead into development of FEM. Free vibration analysis by FEM is performed by solving discretized eigenvalue problem by numerical algorithm such as [2] and good accuracy is achieved, see for example [3], as long as fine enough mesh is used to describe the kinematics of the structure [4]. Due to the fact that the field is mature, numerous application specific recommendations are available for suitable mesh sizes for analysis of thin-walled structures, see for example [5]. Properly discretized model accounts kinematics of all structural length-scales. Such fine mesh approach is applicable for small ships such as superyachts [6] and fishing vessels [7], but not for large cruise ships. Early design of cruise ships needs to account structural optimization including different limit states [8], and to study large geometrical modifications driven by the architecture. Due to these characteristics and limited time available for the design, large ships are still commonly analyzed by utilizing coarse mesh modeling techniques, see Refs. [9, 10]. In ship design, the coarse global model is used for obtaining quasi-static response by use of linear models. The results are then compared against classification rules, which cover the different limit states by closed form expressions for example, buckling, maximum allowed equivalent stress (von Mises) and nominal stresses used for fatigue assessment. Additionally, vibration response analysis is performed to evaluate comfort [11–13], which forms important competitive edge of the ship. This can be done by modal method that utilizes free vibration results. Thus, accuracy and computational effort of the free vibration analysis have central role in the response analysis.

Lowest modes of free vibration of large, lightweight, thin-walled structures, such as cruise ships, are dominated by global length-scale of the structure (Figure 1a) where horizontal and vertical bending as well as torsion are present. However, at higher frequencies, these global modes involve deformations in wide range of interacting structural length-scales (Figure 1b,c). Such modes occur in the frequency range that affect the passenger comfort evaluation. As the local length-scales are deforming all around the large structure, modeling techniques that reduce computational cost in quasi-static analyses by local refinements such as sub-modeling, domain decomposition [14], and global-local [15, 16] methods, are not generally suitable for free vibration analysis [4]. Component-wise method [16–20] can be used for free vibration analysis, and is computationally very effective in comparison with 3D solid models for

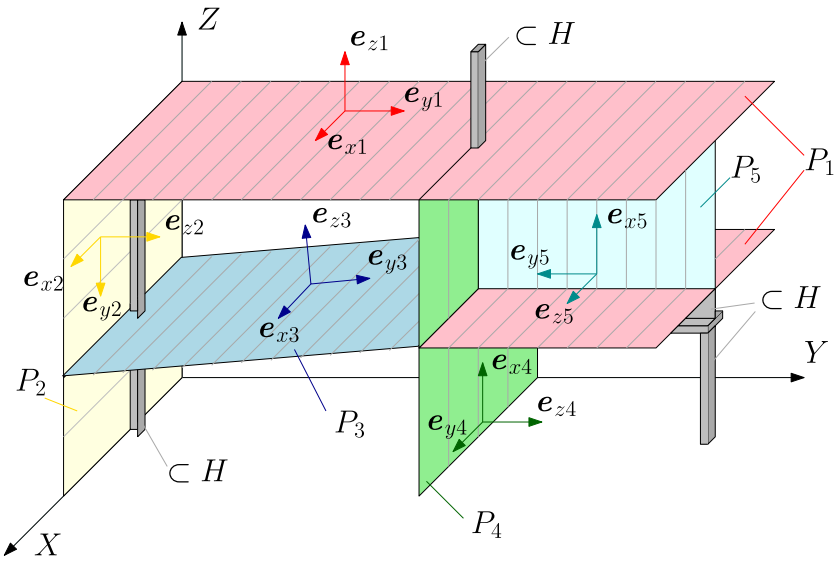

Figure 2. Definition of structure *R* as set of stiffened plates *P* and other structures *H*.

extended 1 D structures. These include structures with varying cross sections, such as aircraft wings [17], simplified ship hull structures [18], civil engineering structures [19], stiffened plates [20] and launchers [21]. However, no benefit was obtained in comparison with shell and beam element models of some thin-walled cases [19].

Another way to reduce FEM models of stiffened thin-walled structures is to combine the smallest structural length-scales by structural homogenization. This can be done by applying equivalent single layer theory (ESL), see for example [8, 22]. This approach is usable for analysis of very large structures and reduces modeling effort and enables faster computation. However, this simplification restraints the natural deformation of the structural system by neglecting deformation of the local plate relative to secondary stiffeners, see Figure 1c. This kinematic restraint causes error in free vibration results [13, 22, 23] as the associated kinetic and strain energy is neglected.

Objective of this paper is to reintroduce effect of this local length-scale deformation and model this energy analytically. Logic similar to the method for 'approximately simple system' in Rayleigh's book [1] is used. ESL-FEM for stiffened plates is used to model the 'simple system'. Locally, plate fields are assumed to deform between stiffeners as they were excited by enforced motion at the modal frequency. Strain and kinetic energies are analytically derived for the complete structure by utilizing global and the local parts of the mode shapes. Iterations are applied to account the dynamic effects at these global, homogenized, and local, analytically solved, discrete length-scales. Similar approach has been successfully applied earlier by the authors to include cross section deformations for beams [24], and local plate deformations for an individual deck [13, 23] and here the extension to general 3-dimensional thin-walled structure is carried out. In order to do so, we also pay attention to the assumed local symmetric and asymmetric wave forms and their inertia effects. The extension adopted is based on assuming that the out-of-plane deformation of the stiffened panel is the primary source of the additional energy and instead of solving the lower length-scale in full 3D. Case study representing part of typical cruise ship superstructure, with stiffened panels oriented at different directions is used to validate the model.

1.1. Definition of large thin-walled structure

Thin-walled structures such as bulkheads and decks are typically metal plates stiffened by primary and secondary stiffeners. Structure *R*, is here considered as a material filled subset of a three-dimensional Euclidean space defined by Cartesian coordinates *X*, *Y*, and *Z*:

$$R \subset \mathbb{R}^3. \tag{1}$$

Let us define that a "stiffened plate P_p" is such subset of planar plates that have unique (in *R*) combination of the following parameters: Material (E_p, ρ_p, ν_p), plate thickness (t_p), uniform secondary stiffener spacing (S_p), nonstructural mass per area ($m_{\mathrm{NS}p}$), and set of orthonormal orientation vectors ($\boldsymbol{e}_{xp}$, $\boldsymbol{e}_{yp}$, $\boldsymbol{e}_{zp}$), see Figure 2. The directional vectors $\boldsymbol{e}_{xp}$, $\boldsymbol{e}_{yp}$, and $\boldsymbol{e}_{zp}$ are pointing in the direction of stiffeners, opposite to that and in the normal direction to the plate respectively. All *N* stiffened plates of the structure form set *P*:

$$P = \bigcup_{p=1}^{N} P_p \subset R. \tag{2}$$

The structure *H* is

$$H = R \setminus P. \tag{3}$$

By this definition, the stiffeners along with all other structures belong to set *H*. The division is to separate structural parts *P* where inertia-induced local plate deformations are considered.

1.2. Vibration modes as generalized single degree of freedom systems

Small amplitude, harmonic, free vibration of linear undamped system, is assumed, see Figure 3. At time t_1 all

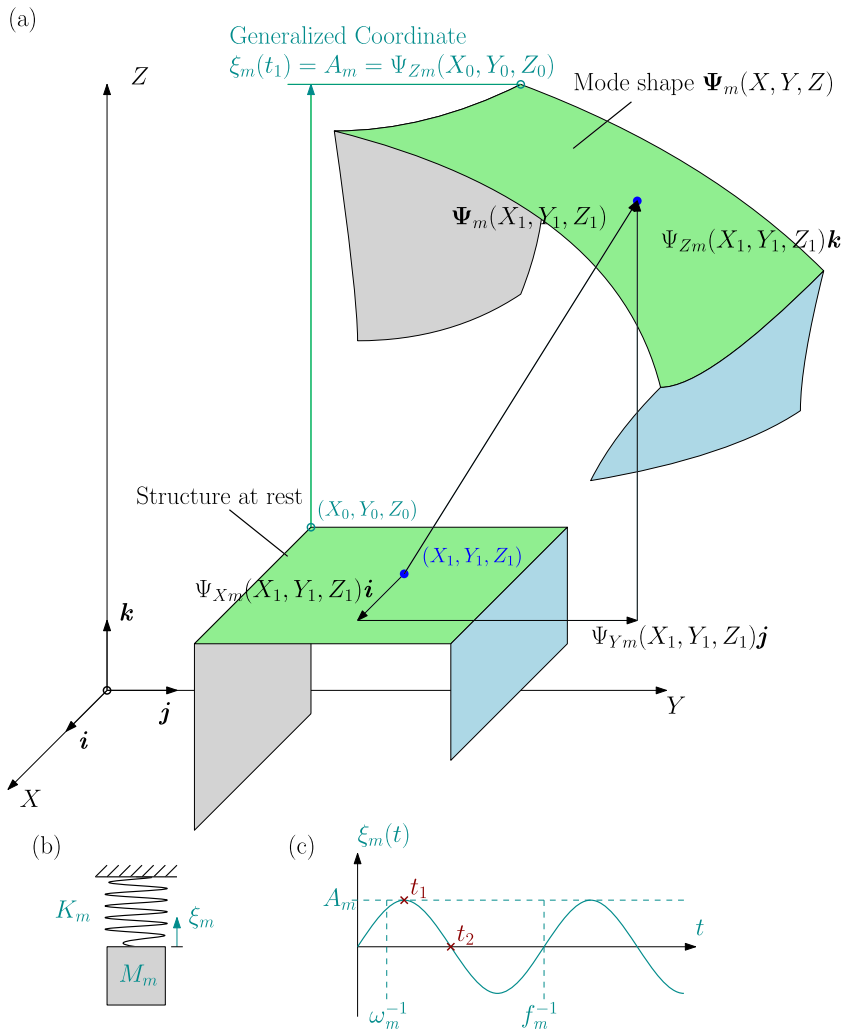

Figure 3. Free vibration of structure at mode m in terms of (a) mode shape, (b) generalized single degree of freedom system, and (c) harmonic motion. Connected together by common generalized coordinate ξ_m (here Z-translation of point (X_0,Y_0,Z_0)).

mechanical energy, E, in the system is in form of strain energy, U, and at moment t_2 in form of kinetic energy, T. The peak values of these energies must be equal and thus,

$$T_m(t_2) = T_m^{\text{peak}} = U_m^{\text{peak}} = U_m(t_1). \tag{4}$$

Free vibration of a structure is defined by its vibration modes. Each mode m represents a dynamic equilibrium state of the structure. Theoretically, infinite number of modes exist for a continuous structure of which only part can be solved by FEM. As the modes are orthogonal [25], they are studied separately. Mode shape, $\boldsymbol{\Psi}_m$, defines displacement relations within the structure. The three-dimensional mode shape function $\boldsymbol{\Psi}_m$ for mode m is defined by its components and global unit vectors as follows:

$$\boldsymbol{\Psi}_m(X, Y, Z) = \Psi_{Xm}(X, Y, Z)\boldsymbol{i} + \Psi_{Ym}(X, Y, Z)\boldsymbol{j} + \Psi_{Zm}(X, Y, Z)\boldsymbol{k},$$
$$(X, Y, Z) \in R. \tag{5}$$

Generalized coordinate, ξ_m, is used as the single degree of freedom, to define generalized system properties for the mode. It is selected as displacement component in freely selected point (X_0,Y_0,Z_0) of the structure with an exception of nodal (zero) points of the mode shape. Motion of the generalized coordinate is written as:

$$\xi_m(t) = A_m \sin(\omega_m t). \tag{6}$$

Generalized mass, M_m, and generalized stiffness K_m are needed to define the generalized system. The kinetic energy in terms of generalized mass is

$$T_m(t) = \frac{1}{2} M_m \dot{\xi}_m(t)^2 = \frac{M_m}{2} [A_m \omega_m \cos(\omega_m t)]^2 \tag{7}$$

and the strain energy in terms of generalized stiffness is

$$U_m(t) = \frac{1}{2} K_m \xi_m(t)^2 = \frac{K_m}{2} [A_m \sin(\omega_m t)]^2. \tag{8}$$

The modal angular frequency can be solved by Eq. (4) by applying peak values of Eqs. (7) and (8) giving:

$$\omega_m = \sqrt{\frac{K_m}{M_m}}. \tag{9}$$

Now, displacement in any point of the structure can be presented by using mode shape and the generalized coordinate as:

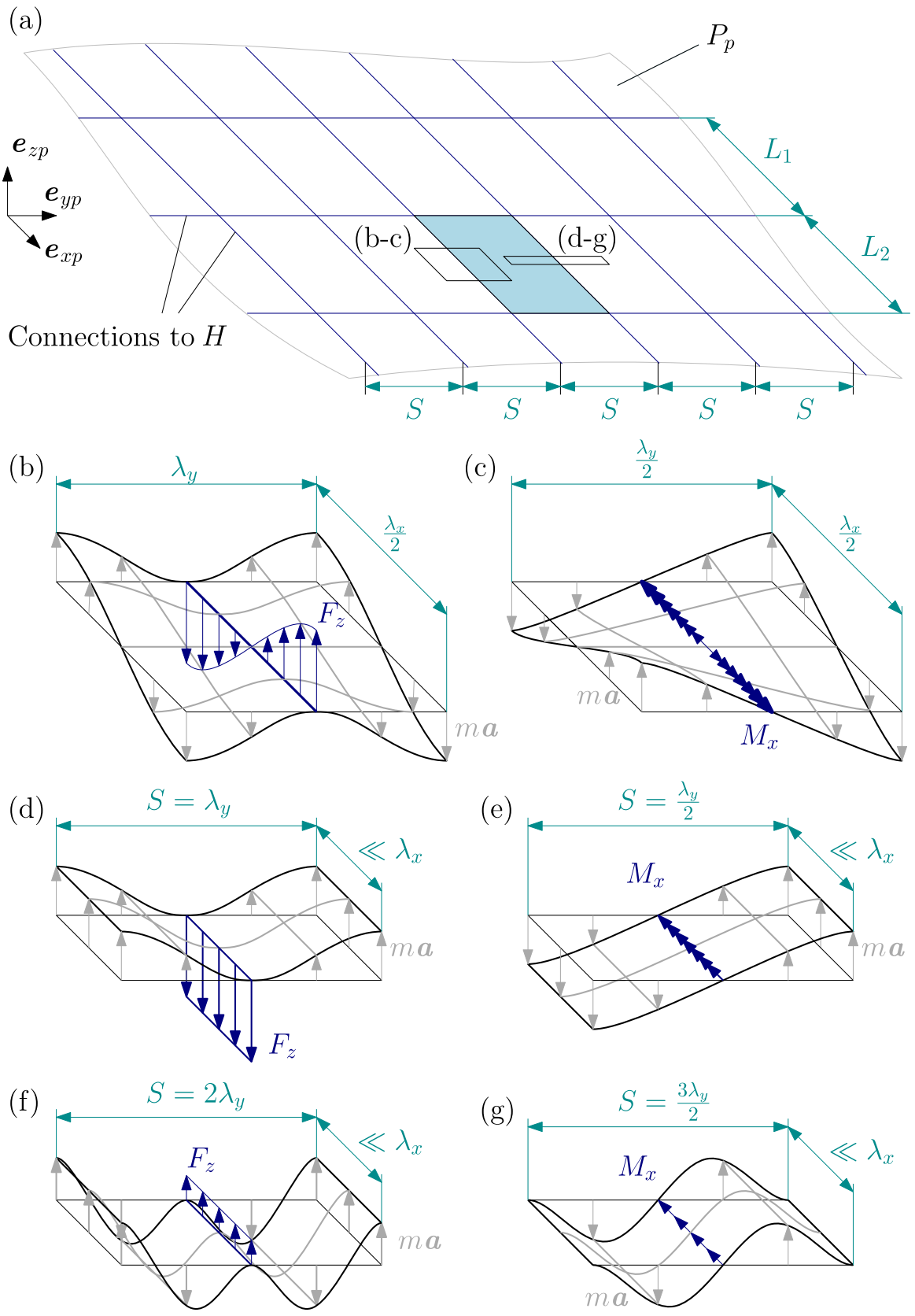

Figure 4. Local deformation waveforms within stiffened plate P_p and their inertia-induced reaction force F_z and moment M_x sketches toward other structures H. (a) Stiffened plate P_p as continuous periodic structure, periodic unit highlighted. (b) Symmetric waveform with short waves in x-direction. (c) Antisymmetric waveform with short waves in x-direction. (d) 1st order symmetric waveform with cylindrical bending assumption. (e) 1st order antisymmetric waveform with cylindrical bending assumption. (f) 2nd order symmetric waveform with cylindrical bending assumption. (g) 2nd order antisymmetric waveform with cylindrical bending assumption.

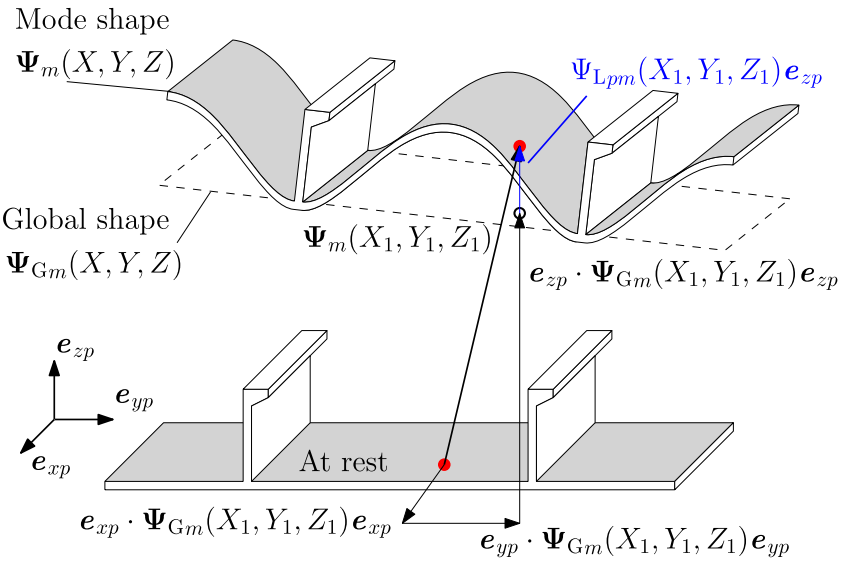

Figure 5. Mode shape $\boldsymbol{\Psi}_m$ in part of panel p. Divided into components parallel to panel orientation vectors. Local plate deformation in blue.

$$\boldsymbol{w}_m(X,Y,Z,t)=\frac{\boldsymbol{\Psi}_m(X,Y,Z)}{A_m}\xi(t)=\boldsymbol{\Psi}_m(X,Y,Z)\sin(\omega_m t). \quad (10)$$

1.3. Local deformation in stiffened plates: assumptions and limitations

It is assumed that local deformation inducing length-scale interaction occurs only in plate normal ($\boldsymbol{e}_{zp}$) direction. This is reasonable assumption for thin-walled structures where out-of-plane deformations are significantly larger than those of in-plane. The plate P_p is assumed to be large enough to be assessed as a continuous periodic structure, see Figure 4a. As presented in [26, 27], a single periodic unit with either symmetric or antisymmetric boundaries at opposite edges can cover all deformation waveforms occurring in such structure. Figure 4b shows waveform of the symmetric case with wavelengths λ_x and λ_y in $\boldsymbol{e}_{xp}$ and $\boldsymbol{e}_{yp}$ directions respectively. The waveform induces normal ($\boldsymbol{e}_{zp}$) reaction force distribution F_z along the length of the stiffener. The distribution follows the wavelength λ_x and changes sign in the nodal (zero) points of the deformation waves. This waveform would induce highest resultant reaction forces when the (global) mode shape matches the local wavelength λ_x. We focus here to global modes with long waves relative to S. In case of short local λ_x wavelengths, reaction force resultant over a much longer global wave would approach to zero. As a consequence, such waveforms will interact very little with larger length-scales. Similar reasoning applies for the antisymmetric waveform presented in Figure 4c. As a difference, the reaction between P_p and H is moment distribution M_x around $\boldsymbol{e}_{xp}$ instead of the force distribution of the symmetric case. Therefore, we focus on local waveforms with long local waves in $\boldsymbol{e}_{xp}$ direction. The longest possible local wave is either length of one or two periodic units, depending on waveform boundaries in the short edges of the periodic unit. Cylindrical bending approximation is introduced to overcome this challenging dependency and to enable the local waveform to follow wavelengths of global mode shapes. This is reasonable approximation for plates with aspect ratios $L/S>3$ [28]. Length of local flexural waves in $\boldsymbol{e}_{yp}$ direction is considered next. Figure 4d,f represent two lowest order symmetric waveforms, and Figure 4e,g two lowest order antisymmetric waveforms. Symmetric waveforms are inducing reaction forces between P_p and H, while antisymmetric waveforms induce moments. Reaction moments of the antisymmetric waveforms have opposite signs in adjacent stiffeners. In case of long global waves in $\boldsymbol{e}_{yp}$ direction, resultant of these reaction moments over the global wave approaches zero. These antisymmetric local waveforms can thus be neglected and symmetric waveforms that induce out of plane reaction forces remain. From those, the first order waveform of Figure 4d is the most significant. So, second order, Figure 4f, and higher order symmetric waveforms are assumed negligible in this study.

With these assumptions the objective is to develop a calculation method that includes only first order symmetric waveforms of local deformation in the free vibration of large thin-walled structures. This causes the inertia-induced length-scale interaction.

2. Method definition

2.1. Mode shape as combination of global and local deformations

The mode shape (5) can be written as:

$$\boldsymbol{\Psi}_m(X,Y,Z)=\begin{cases}\left[\boldsymbol{e}_{xp}\cdot\boldsymbol{\Psi}_m(X,Y,Z)\right]\boldsymbol{e}_{xp}+\left[\boldsymbol{e}_{yp}\cdot\boldsymbol{\Psi}_m(X,Y,Z)\right]\boldsymbol{e}_{yp}\\ +\left[\boldsymbol{e}_{zp}\cdot\boldsymbol{\Psi}_m(X,Y,Z)\right]\boldsymbol{e}_{zp},(X,Y,Z)\in P\\ \boldsymbol{\Psi}_m(X,Y,Z),(X,Y,Z)\in H.\end{cases} \quad (11)$$

The mode shape is divided into global mode shape coinciding with the plane of stiffener-plate connections, and local deformation occurring between the stiffeners, see Figure 5.

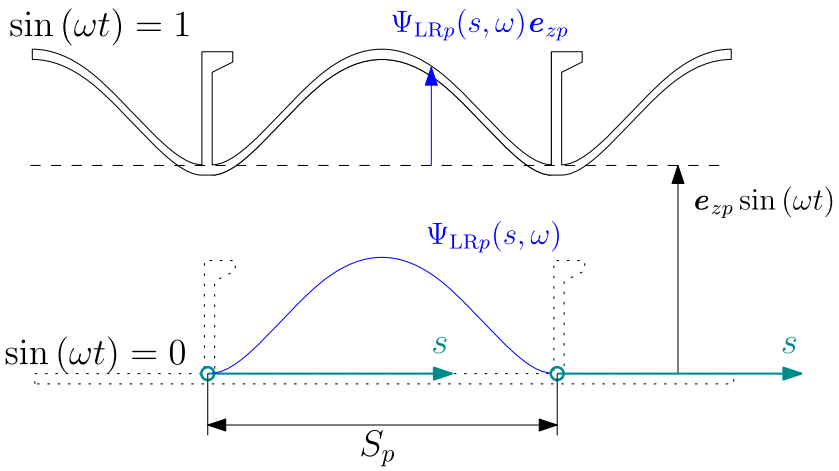

Figure 6. Relative local bending as function of local coordinate *s*.

Normal component is then:

$$\boldsymbol{e}_{zp} \cdot \boldsymbol{\Psi}_m(X,Y,Z) = \boldsymbol{e}_{zp} \cdot \boldsymbol{\Psi}_{\mathrm{G}m}(X,Y,Z) + \Psi_{\mathrm{L}pm}(X,Y,Z), \tag{12}$$

where $\boldsymbol{\Psi}_{\mathrm{G}m}$, and $\Psi_{\mathrm{L}pm}$ represents global and local parts of the mode shape respectively. Due to linearity of the system, the local part can be written as product of global mode shape normal component $\boldsymbol{e}_{zp}\cdot\boldsymbol{\Psi}_{\mathrm{G}m}$, and relative deformation response shape $\Psi_{\mathrm{LR}p}$ of the local plate. Thus, the local deformation is:

$$\Psi_{\mathrm{L}pm}(X,Y,Z,s,\omega_m) = \left[\boldsymbol{e}_{zp} \cdot \boldsymbol{\Psi}_{\mathrm{G}m}(X,Y,Z)\right]\Psi_{\mathrm{LR}p}(s,\omega_m). \tag{13}$$

The panel P_p normal component of mode shape becomes:

$$\boldsymbol{e}_{zp} \cdot \boldsymbol{\Psi}_m(X,Y,Z,s,\omega_m) = \boldsymbol{e}_{zp} \cdot \boldsymbol{\Psi}_{\mathrm{G}m}(X,Y,Z)\left[1 + \Psi_{\mathrm{LR}p}(s,\omega_m)\right]. \tag{14}$$

It was assumed that the local deformation occurs only in direction normal to the stiffened panels *P*. Then, the mode shape of the whole structure can be written as:

$$\boldsymbol{\Psi}_m(X,Y,Z,s,\omega_m) = \begin{cases} \left[\boldsymbol{e}_{xp} \cdot \boldsymbol{\Psi}_{\mathrm{G}m}(X,Y,Z)\right]\boldsymbol{e}_{xp} + \left[\boldsymbol{e}_{yp} \cdot \boldsymbol{\Psi}_{\mathrm{G}m}(X,Y,Z)\right]\boldsymbol{e}_{yp} \\ +\left[\boldsymbol{e}_{zp} \cdot \boldsymbol{\Psi}_{\mathrm{G}m}(X,Y,Z)\right]\left[1 + \Psi_{\mathrm{LR}p}(s,\omega_m)\right]\boldsymbol{e}_{zp}, (X,Y,Z) \in P \\ \boldsymbol{\Psi}_{\mathrm{G}m}(X,Y,Z), (X,Y,Z) \in H. \end{cases} \tag{15}$$

where global mode shapes $\boldsymbol{\Psi}_{\mathrm{G}m}$ of Eq. (15) are solved with homogenized ESL, see for example [29–32].

2.2. Global mode shapes by finite element method

The mode shapes are solved with FEM as a list of discrete nodal translation and rotation values, by solving:

$$[M]\{\ddot{w}_{\mathrm{G}}\} + [K]\{w_{\mathrm{G}}\} = [0], \tag{16}$$

where M is the global mass, and K the global stiffness matrix. The solution can be obtained by using the equivalent single layer (ESL) theory [22] and [23], see Figure 1b. Stiffness matrix formulation for these elements is summarized in Appendix A. The division of mass can be done by lumped or consistent approach. In lumped approach, element's mass is divided based on its static geometry between the nodes, leading to diagonal mass matrix. In consistent approach [33], the mass is divided by utilizing elemental shape functions as used in stiffness matrix generation, leading to non-diagonal matrix. In case of very coarse mesh relative to deformation wavelengths, the resulting improvement in accuracy can be significant even though computational effort increases. Then Eq. (16) can be solved from:

$$\left[K - \omega_{\mathrm{G}m}^2 M\right]\{\Psi_{\mathrm{G}m}\} = [0]. \tag{17}$$

Lanczos [2] is used to solve the problem. The FEM mode shapes are normalized so that FEM generalized mass of the mode in question equals unity.

2.3. Relative local deformations by enforced response

Relative local bending shape function $\Psi_{\mathrm{LR}p}(s,\ \omega)$ for symmetric waveform of local deformation can be obtained by forced vibration analysis of the local unit, that is a plate field between stiffeners. The local model is excited by unit amplitude enforced support motion. Here we use analytical formulae from textbooks [34, 35]. This simple method is applicable for structures where cylindrical bending and clamped-clamped boundary conditions can be assumed, see Figure 6. Local coordinate *s* is defined as distance from stiffener in $\boldsymbol{e}_{yp}$ direction.

Mode shape is given analytically in [34] and can be written as:

$$\Psi_{\mathrm{LR}p}(s,\omega) = \frac{r_{\mathrm{d}p}(\omega)}{B}\left[\sigma\sin\left(\frac{\beta s}{S_p}\right) - \sigma\sinh\left(\frac{\beta s}{S_p}\right) - \cos\left(\frac{\beta s}{S_p}\right) + \cosh\left(\frac{\beta s}{S_p}\right)\right], \tag{18}$$

where $\sigma \approx 0.982502215$ and $\beta \approx 4.73004074$ are tabulated parameter values from [34]. Normalization factor B is solved by setting mid span response equal to dynamic response in that point $r_{\mathrm{d}p}$. It follows:

$$B = \sigma\sin\left(\frac{\beta}{2}\right) - \sigma\sinh\left(\frac{\beta}{2}\right) - \cos\left(\frac{\beta}{2}\right) + \cosh\left(\frac{\beta}{2}\right). \tag{19}$$

Dynamic response of the mid span $r_{\mathrm{d}p}(\omega)$ can be written as dynamically amplified static response $r_{\mathrm{s}p}$ as follows:

$$r_{dp}(\omega) = \left(1 - \frac{\omega}{\omega_{Lp}}\right)^{-1} r_{sp}(\omega), \tag{20}$$

where modal frequency of the clamped-clamped lowest mode ω_{Lp} is [34]:

$$\omega_{Lp} = \frac{\beta^2}{{S_p}^2}\sqrt{\frac{D_p}{m_p}}. \tag{21}$$

Static response r_{sp} can be found by considering static bending in mid span that uniform inertia load of unit amplitude motion would cause [35]:

$$r_{sp}(\omega) = \frac{m_p \omega^2 {S_p}^4}{384 D_p}. \tag{22}$$

where the plate bending stiffness D_p is

$$D_p = \frac{{t_p}^3 E_p}{12(1-{\upsilon_p}^2)}, \tag{23}$$

and t_p, E_p and ν_p are the plate thickness, Young's modulus and Poisson's ratio respectively. The mass for unit area of plate:

$$m_p = t_p \rho_p + m_{NSp}, \tag{24}$$

where ρ_p is material density and m_{NSp} nonstructural mass per area.

2.4. Generalized mass from kinetic energy

The generalized mass of mode m can be found by considering the peak value of kinetic energy of the vibration mode, that is when $\cos(\omega_m t) = 1$, see Figure 3c. The generalized mass is solved from Eq. (7) as:

$$M_m = \frac{2T_m^{peak}}{{A_m}^2 {\omega_m}^2}. \tag{25}$$

Total kinetic energy T_m can be written as sum of translational kinetic energy of the stiffened plates T_{Pm} and all other kinetic energy of the structure T_{Hm} as

$$T_m(\omega_m, t) = T_{Hm}(\omega_m, t) + T_{Pm}(\omega_m, t). \tag{26}$$

The term T_H in Eq. (26) represents the kinetic energy that does not depend directly on the local deformation parts of the mode shape. However, it is considered as function of frequency because the velocity changes with the frequency, see Chapter 2.6. Translational kinetic energy of stiffened plates T_{Pm} is a sum of translation kinetic energies of all N stiffened plates:

$$T_{Pm}(\omega_m, t) = \sum_{p=1}^{N} \oiint_{Pp} \left(\frac{1}{2} m_p \left\{ \frac{\partial \left[\boldsymbol{\Psi}_m(X,Y,Z) \sin(\omega_m, t) \right]}{\partial t} \right\}^2 \right). \tag{27}$$

Peak value of which occurs when $\cos(\omega_m t)=1$ giving:

$$T_{Pm}^{peak}(\omega_m) = \frac{{\omega_m}^2}{2} \sum_{p=1}^{N} \oiint_{Pp} \left\{ m_p [\boldsymbol{\Psi}_m(X,Y,Z)]^2 \right\}. \tag{28}$$

Now by applying mode shape of Eq. (15) gives

$$T_{Pm}^{peak}(\omega_m) = \frac{{\omega_m}^2}{2} \sum_{p=1}^{N} \oiint_{Pp} \left(m_p \left\{ \left[\boldsymbol{e}_{xp} \cdot \boldsymbol{\Psi}_{Gm}(X,Y,Z) \right] \boldsymbol{e}_{xp} + \left[\boldsymbol{e}_{yp} \cdot \boldsymbol{\Psi}_{Gm}(X,Y,Z) \right] \boldsymbol{e}_{yp} + \left[\boldsymbol{e}_{zp} \cdot \boldsymbol{\Psi}_{Gm}(X,Y,Z) \frac{1}{S_p} \int_0^{S_p} 1 + \Psi_{LRp}(s, \omega_m) ds \right] \boldsymbol{e}_{zp} \right\}^2 \right). \tag{29}$$

Panel orientation vectors are orthonormal giving:

$$T_{Pm}^{peak}(\omega_m) = \frac{{\omega_m}^2}{2} \sum_{p=1}^{N} \oiint_{Pp} \left(m_p \left\{ \left[\boldsymbol{e}_{xp} \cdot \boldsymbol{\Psi}_{Gm}(X,Y,Z) \right]^2 + \left[\boldsymbol{e}_{yp} \cdot \boldsymbol{\Psi}_{Gm}(X,Y,Z) \right]^2 + \left[\boldsymbol{e}_{zp} \cdot \boldsymbol{\Psi}_{Gm}(X,Y,Z) \right]^2 \left[\frac{1}{S_p} \int_0^{S_p} 1 + \Psi_{LRp}(s, \omega_m) ds \right]^2 \right\} \right). \tag{30}$$

The term independent of global mode shape in Eq. (30) represents property of the stiffened plate P_p. and is called "relative local response coefficient" of the panel:

$$c_{LRp}(\omega) = \frac{1}{S_p} \left(\int_0^{S_p} \left[1 + \Psi_{LRp}(s, \omega) \right] ds \right)^2. \tag{31}$$

The relative local response coefficient c_{LR} can be solved by inserting local relative deformation shape of Eq. (18). Now the peak kinetic energy can be written as:

$$T_m^{peak}(\omega_m) = T_{Hm}^{peak}(\omega_m) + \frac{{\omega_m}^2}{2} \sum_{p=1}^{N} \oiint_{Pp} \left(m_p \left\{ \left[\boldsymbol{e}_{xp} \cdot \boldsymbol{\Psi}_{Gm}(X,Y,Z) \right]^2 + \left[\boldsymbol{e}_{yp} \cdot \boldsymbol{\Psi}_{Gm}(X,Y,Z) \right]^2 + \left[\boldsymbol{e}_{zp} \cdot \boldsymbol{\Psi}_{Gm}(X,Y,Z) \right]^2 c_{LRp}(\omega_m) \right\} \right). \tag{32}$$

By inserting Eq. (32) into Eq. (25), generalized mass is:

$$M_m = \frac{2T_{Hm}^{peak}(\omega_m)}{{A_m}^2 {\omega_m}^2} + \frac{1}{{A_m}^2} \sum_{p=1}^{N} \oiint_{Pp} \left(m_p \left\{ \left[\boldsymbol{e}_{xp} \cdot \boldsymbol{\Psi}_m(X,Y,Z) \right]^2 + \left[\boldsymbol{e}_{yp} \cdot \boldsymbol{\Psi}_m(X,Y,Z) \right]^2 + \left[\boldsymbol{e}_{zp} \cdot \boldsymbol{\Psi}_{Gm}(X,Y,Z) \right]^2 c_{LRp}(\omega_m) \right\} \right). \tag{33}$$

The resulting definition for generalized mass is in FEM context:

$$M_m(\omega_m) = \frac{2T_{Hm}^{peak}(\omega_m)}{{A_m}^2 {\omega_m}^2} + \frac{1}{{A_m}^2} \sum_{p=1}^{N} \sum_{n \in P_p} \left\{ m_p \alpha_n \left[\left(\boldsymbol{e}_{xp} \cdot \boldsymbol{\Psi}_{Gmn} \right)^2 + \left(\boldsymbol{e}_{yp} \cdot \boldsymbol{\Psi}_{Gmn} \right)^2 + \left(\boldsymbol{e}_{zp} \cdot \boldsymbol{\Psi}_{Gmn} \right)^2 c_{LRp}(\omega_m) \right] \right\}. \tag{34}$$

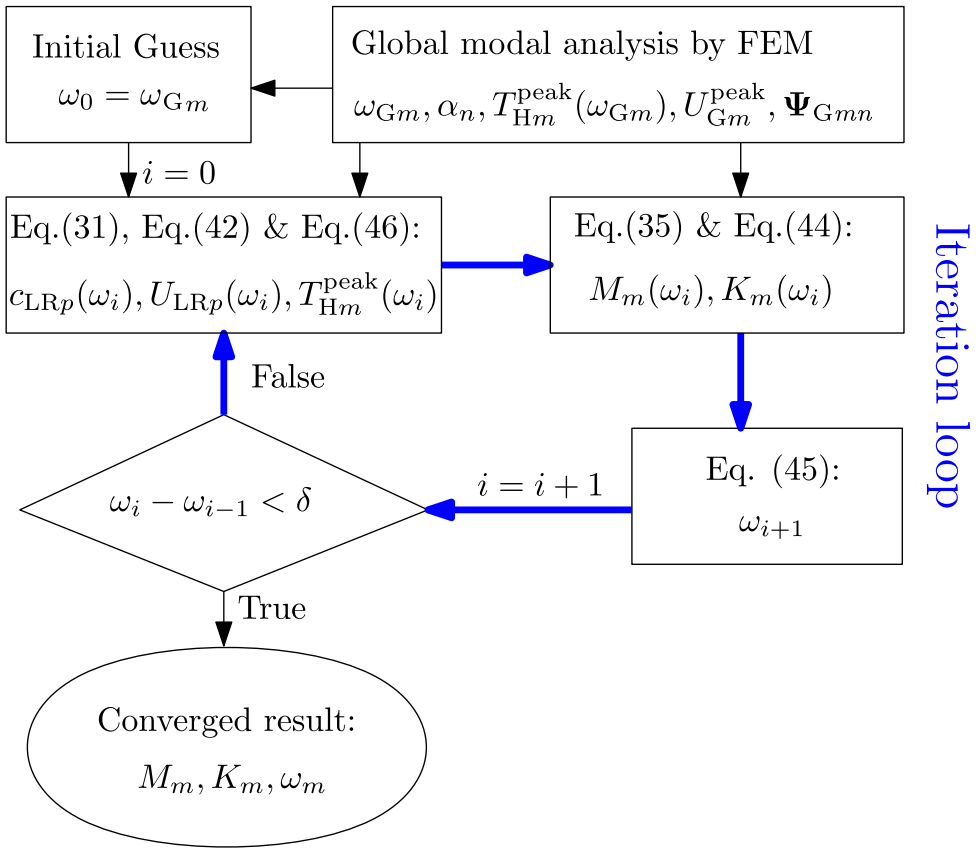

Figure 7. Flow chart of the iterative process for modal properties.

where integrals have been replaced by summations. In Eq. (34), mass of the plate is divided to nodes by area α_n of plate assigned to node n, (similar to lumped mass FEM approach). Ψ_{Gmn} are the nodal translation values of the global mode m shape vector in node n. For practical application, it is beneficial to take relative local response coefficient outside the inner summation of Eq. (34) by partitioning the sum as follows:

$$M_m(\omega_m) = \frac{2T_{Hm}^{peak}(\omega_m)}{{A_m}^2{\omega_m}^2} + \frac{1}{{A_m}^2}\sum_{p=1}^{N}\left(m_p\left\{\sum_{n\in P_p}\left[\alpha_n\left(\boldsymbol{e}_{xp}\cdot\Psi_{Gmn}\right)^2\right] + \sum_{n\in P_p}\left[\alpha_n\left(\boldsymbol{e}_{yp}\cdot\Psi_{Gmn}\right)^2\right] + c_{LRp}(\omega_m)\sum_{n\in P_p}\left[\alpha_n\left(\boldsymbol{e}_{zp}\cdot\Psi_{Gmn}\right)^2\right]\right\}\right). \quad (35)$$

2.5. Generalized stiffness from strain energy

Generalized stiffness K_m of mode m is considered. The definition of strain energy U_m for generalized single degree of freedom system (Figure 3b) is given in Eq. (8). All energy of the considered system is in form of strain energy when $\sin(\omega_m t) = 1$, for example, t_1 in Figure 3c. Generalized stiffness can now be solved as function of the peak strain energy, giving:

$$K_m = \frac{2}{{A_m}^2}U_m^{peak}. \quad (36)$$

Strain energy in Eq. (36) is a sum of strain energy of local deformation in P, U_{Lm}, and a global deformation strain energy U_{Gm}. The global term U_{Gm} includes all strain energy of the structure R mode m as solved with the global model (Chapter 2.2). The strain energy as function of time is:

$$U_m(\omega_m, t) = \left[U_{Lm}^{peak}(\omega_m) + U_{Gm}^{peak}\right]\sin(\omega_m t). \quad (37)$$

Peak values occur when $\sin(\omega_m t) = 1$:

$$U_m^{peak}(\omega_m) = U_{Lm}^{peak}(\omega_m) + U_{Gm}^{peak}. \quad (38)$$

In Eq. (38) peak strain energy of the local deformation needs closer consideration:

$$U_{Lm}^{peak}(\omega_m) = \frac{1}{2}\sum_{p=1}^{N}\oiint_{P_p}\left\{\frac{D_p}{S_p}\int_0^{S_p}\left[\frac{\partial^2\Psi_{Lpm}(X,Y,Z,s_p,\omega_m)}{\partial {s_p}^2}\right]^2 ds_p\right\}. \quad (39)$$

Local deformation shape can be written as product of global, and relative local terms as done in Eq. (13) giving:

$$U_{Lm}^{peak}(\omega_m) = \frac{1}{2}\sum_{p=1}^{N}\oiint_{P_p}\left(\frac{D_p}{S_p}\int_0^{S_p}\left\{\frac{\partial^2\left[\boldsymbol{e}_{zp}\cdot\Psi_{Gm}(X,Y,Z)\Psi_{LRp}(s_p,\omega_m)\right]}{\partial {s_p}^2}\right\}^2 ds_p\right). \quad (40)$$

Local relative deformation Ψ_{LRp} is not function of the location within the panel P_p, but general parameters of it. Thus, the integrals can be separated into:

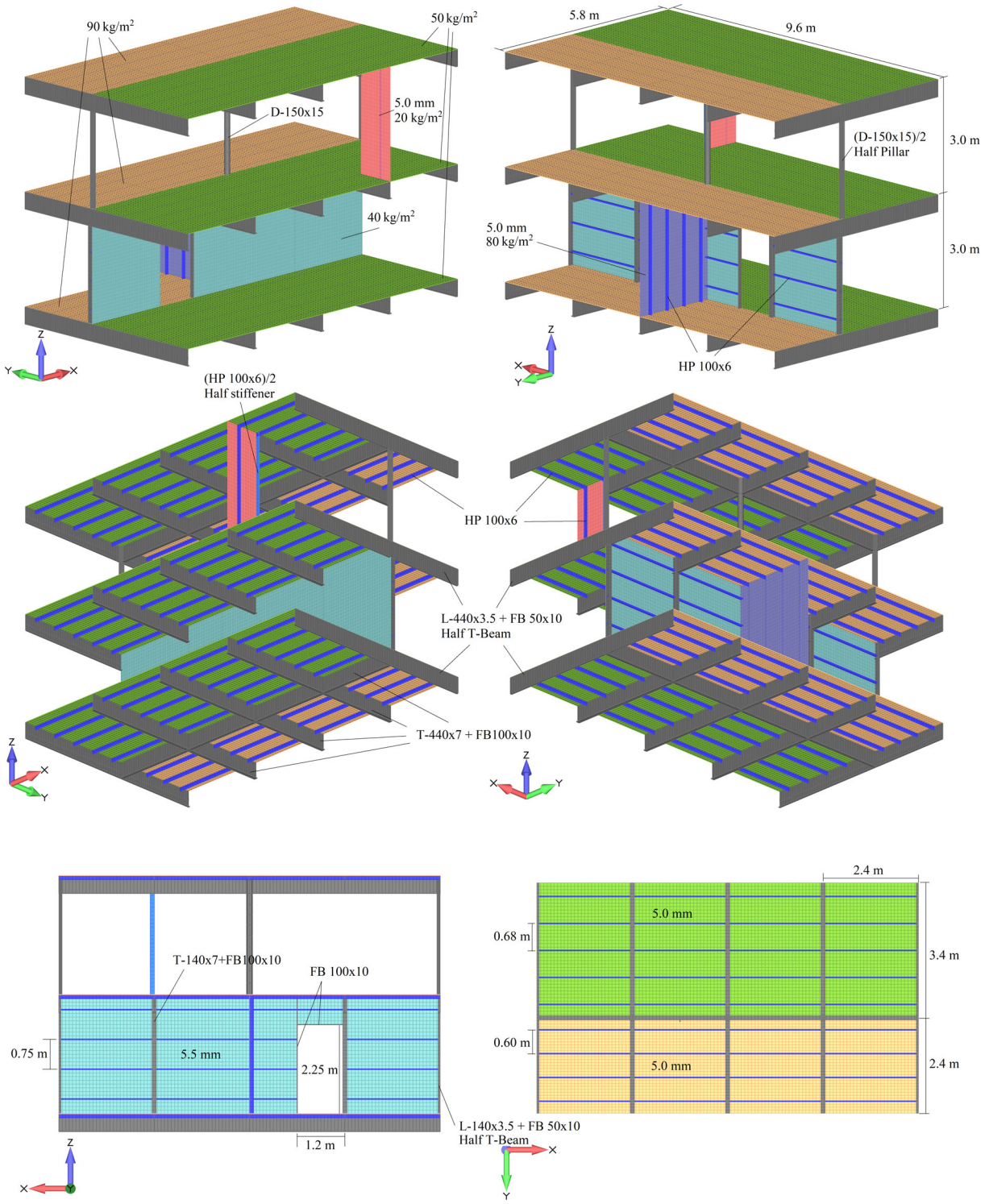

Figure 8. Structure for the case study.

$$U_{\mathrm{Lm}}^{\mathrm{peak}}(\omega_m) = \frac{1}{2}\sum_{p=1}^{N}\left\{\frac{D_p}{S_p}\int_0^{S_p}\left[\frac{\partial^2 \Psi_{\mathrm{LR}p}(s_p,\omega_m)}{\partial {s_p}^2}\right]^2 ds_p \iint_{P_p}\left[\boldsymbol{e}_{zp}\cdot\boldsymbol{\Psi}_{\mathrm{G}m}(X,Y,Z)\right]^2\right\}. \tag{41}$$

Let us define factor $U_{\mathrm{LR}p}$ as peak strain energy of unit area of panel P_p under enforced excitation of unit amplitude of the global reference plane.

$$U_{\mathrm{LR}p}(\omega) = \frac{D_p}{2S_p}\int_0^{S_p}\left[\frac{\partial^2 \Psi_{\mathrm{LR}p}(s,\omega)}{\partial s^2}\right]^2 ds. \tag{42}$$

Generalized stiffness of Eq. (36) can now be written:

$$K_m(\omega_m) = \frac{2}{{A_m}^2}\left(U_{\mathrm{G}m}^{\mathrm{peak}} + \sum_{p=1}^{N}\left\{U_{\mathrm{LR}p}(\omega_m)\iint_{P_p}\left[\boldsymbol{e}_{zp}\cdot\boldsymbol{\Psi}_{\mathrm{G}m}(X,Y,Z)\right]^2\right\}\right). \tag{43}$$

Application with Discretized global mode shape by FEM is done similarly as in Eq. (34). Eq. (43) gets the form:

$$K_m(\omega_m) = \frac{2}{{A_m}^2}\left\{ U_{Gm}^{peak} + \sum_{p=1}^{N}\left[U_{LRp}(\omega_m) \sum_{n\in P_p} \alpha_n \left(\boldsymbol{e}_{zp} \cdot \boldsymbol{\Psi}_{Gmn} \right)^2 \right] \right\}. \quad (44)$$

Table 1. Stiffened plates of the case study structure.

Index p	Structure	Plate t_p	Spacing S_p	Ratio L/S	Nonstructural mass m_{NSp}	$\mathbf{e}_{xp}$	$\mathbf{e}_{yp}$	$\mathbf{e}_{zp}$
1	Decks 1	5.0 mm	0.68 m	3.52	50 kgm^{-2}	**i**	**j**	**k**
2	Decks 2	5.0 mm	0.60 m	4	90 kgm^{-2}	**i**	**j**	**k**
3	Ln Bhd	5.5 mm	0.75 m	3.2	40 kgm^{-2}	**i**	**k**	**j**
4	Tr Bhd 1	5.0 mm	0.60 m	5	80 kgm^{-2}	**k**	**j**	**i**
5	Tr Bhd 2	5.0 mm	0.68 m	4.41	20 kgm^{-2}	**k**	**-j**	**-i**

2.6. Natural frequency by iteration

Now when the generalized mass, Eq. (35), and generalized stiffness, Eq. (44), are known, and the modal natural frequencies could be solved from Eq. (9). However, generalized mass and stiffness are functions of the frequency itself, due to local deformation being a function of the modal frequency. Iterative approach illustrated in Figure 7 is applied to overcome the issue. Angular frequency is solved for each mode with iterative process, where frequency for each iteration step is solved from Eq. (45):

$$\omega_{i+1} = \sqrt{\frac{K_m(\omega_i)}{M_m(\omega_i)}}. \quad (45)$$

In Eq. (35) Kinetic energy T_H is also a function of frequency, because velocity in definition of kinetic energy is a function of frequency. So, the kinetic energy changes with

Table 2. Natural Frequencies and similarity of global plane mode shapes by R^2 estimators of the 10 lowest modes.

Mode #	1	2	3	4	5	6	7	8	9	10
ESL [Hz]	16.185	18.361	18.776	19.029	19.559	19.781	20.329	20.530	21.508	21.936
(vs. shell [%])	(4.52)	(6.00)	(6.60)	(6.80)	(7.20)	(7.23)	(7.73)	(7.71)	(9.96)	(9.48)
Present [Hz]	15.484	17.326	17.615	17.818	18.251	18.455	18.874	19.053	19.834	20.132
(vs. shell [%])	(-0.01)	(0.02)	(0.01)	(0.01)	(0.03)	(0.04)	(0.02)	(-0.04)	(1.40)	(0.48)
Shell [Hz]	15.486	17.322	17.613	17.817	18.245	18.447	18.870	19.061	19.559	20.036
Global plane R^2	0.999	0.995	0.996	0.996	0.997	0.995	0.991	0.988	0.861	0.862

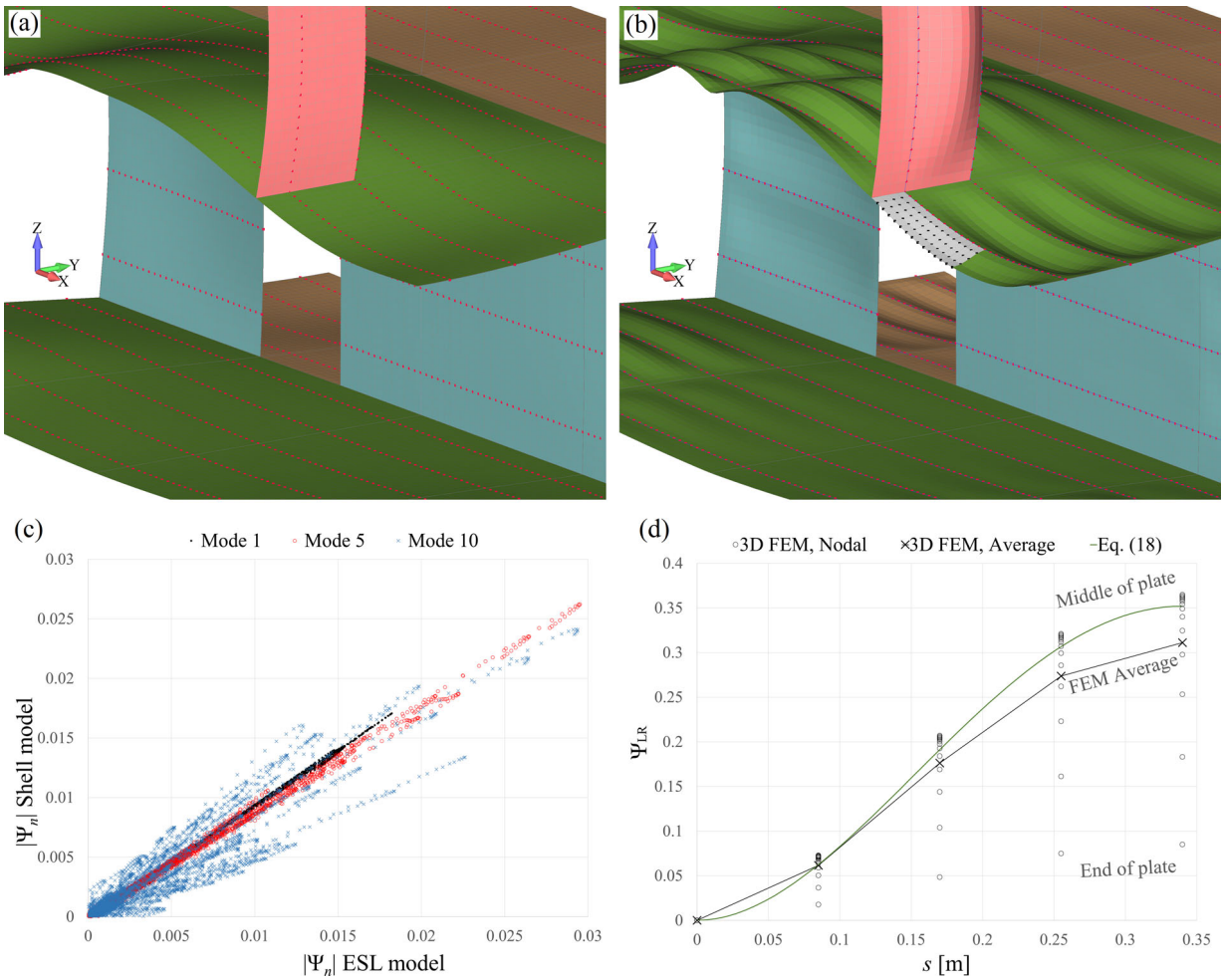

Figure 9. Comparison of mode shapes: (a) Mode 5 by ESL model V. (b) Mode 5 by Shell model. (c) Mode 1, 5 and 10 shape comparisons in stiffener nodes visualized in (a) and (b); shell model result as function of ESL model result. (d) Local shape comparison of highlighted area in (b) between 3D FEM and Eq. (18).

Table 3. Rectangular element sizes in way of the stiffened panels, $\mathbf{e}_x/\mathbf{e}_y$ in mm.

	Model A	Model B	Model C	Model D	Model E	Model F	Model G	Model V	Shell
P_1	1200/1133	800/850	600/567	400/378	300/309	200/200	150/148	86/85	86/85
P_2	1200/1200	800/800	600/600	400/400	300/300	200/200	150/150	86/75	86/75
P_3	1200/1000	800/750	600/600	400/375	300/300	200/200	150/150	86/94	86/94
P_4	1000/1200	750/800	600/600	375/400	300/300	200/200	150/150	94/75	94/75
P_5	1000/1020	750/1020	600/510	375/340	300/340	200/204	150/146	94/85	94/85

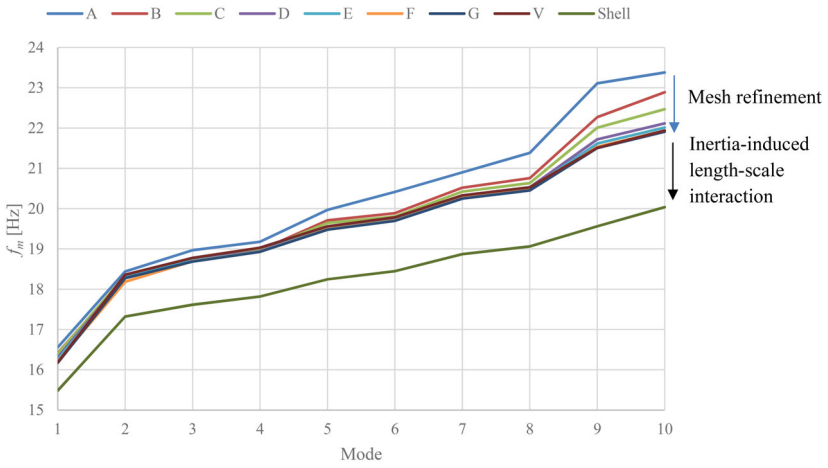

Figure 10. Natural frequencies of the 10 lowest modes by ESL models with different mesh sizes, and the shell model.

Table 4. Modes found and respective solver times for 3 frequency ranges by FE models with various mesh sizes.

	#DOF	0–20 Hz # Modes	0–20 Hz Time [s]	0–30 Hz # Modes	0–30 Hz Time [s]	0–40 Hz # Modes	0–40 Hz Time [s]
Model A	1164	6	0.507	19	0.507	29	0.521
Model B	2238	7	0.542	21	0.568	37	0.586
Model C	3996	7	0.597	22	0.628	42	0.704
Model D	8736	7	0.746	22	0.833	49	0.985
Model E	14346	7	0.925	24	1.098	50	1.339
Model F	32040	7	1.551	24	1.891	50	2.621
Model G	56700	7	2.354	24	3.17	51	4.375
Model V	176064	7	7.462	24	10.177	52	15.765
Shell	176064	10	11.875	160	25.287	293	40.111

the frequency accordingly as follows:

$$T_{\mathrm{H}m}^{\mathrm{peak}}(\omega_{i+1}) = \frac{\omega_i^2}{\omega_{\mathrm{G}}^2} T_{\mathrm{H}m}^{\mathrm{peak}}(\omega_{\mathrm{G}}). \tag{46}$$

3. Case study

3.1. Structure for case study

Structure for validation case study is selected so that it includes structural components typical for cruise ship superstructure. Stiffened plates appear as decks, and as transversal- and longitudinal bulkheads, see Figure 8. Additionally, the structure includes Pillars (D150x15), T-girders in decks (T-440 × 7 + FB100x10) and bulkheads (T-140 × 7 + FB100x10), and large opening (2.25 m x 1.2 m) in the longitudinal bulkhead with flat bar stiffener (FB100x10) on its edges. These are modeled by beam elements (PBEAM in Nastran). Material properties of typical steel are applied for all structural parts: $E = 206$ GPa, $\nu = 0.3$, and $\rho = 7850$ kgm^{-2}.

In lengthwise (X-) direction, the structure is 9.6 meters long, divided by transversal T-girders into four 2.4 m spans. Transversally (Y-direction), the structure is 5.8 meters wide including four 0.6 m and five 0.68 m stiffener spacings. Vertically the structure includes three decks spaced 3 meters apart. Symmetry is applied on the edges of the structure so that it behaves, as it was a part of a larger structure. This symmetry condition is created by including only half of the members on the edges of the structure, and by applying following nodal constraints: Translations in X and Rotations around Y and Z are fixed in edges $X = 0$ and $X = 9.6$ m, and Translation in Y direction and rotations around X and Z are fixed in edges $Y = 0$ and $Y = 5.8$ m. No constraint is applied in Z-direction. The structure includes five stiffened plates listed in Table 1. All secondary stiffeners are considered as small T-sections (T-90 × 6 + FB23x10).

3.2. Results

Present method is validated by comparison with 'Shell model' that includes plates as (PSHELL in Nastran) and secondary stiffeners as offset beams (PBEAM in Nastran) in their geometrical locations. Eight elements between adjacent stiffeners is used. Equivalent single layer model for validation (Model V) is created by using identical mesh in terms of node locations. Only difference is that Equivalent shell elements (PCOMP in Nastran) are used to model the stiffened plates, see Ref. [22] and Appendix A for details. This model is used for obtaining global reference plane mode shapes for the present method.

Lanczos based algorithm SOL 103 of NX Nastran 11.0.2® with lumped mass matrix is used. One zero mode is found

for both models (rigid body mode in Z-direction), these are not considered further.

Natural frequencies of the first 10 nonzero modes are presented in Table 2. The frequencies range from 16.185 to 21.936 Hz for the ESL model, and 15.486 to 20.036 Hz for the Shell model. The obtained frequencies are very close to the shell model results, ranging from 15.484 to 20.132 Hz. The error in frequency against shell model is for the uncorrected ESL $4.5-10\%$, and for the present corrected method $0-1.4\%$.

Comparison of mode shapes is presented in Figure 9. Similarity of global mode shapes are studied by the nodal values in global nodes (shown in Figure 9a,b) between the models. Exactly matching shapes would appear as linear relation in the comparison plot of Figure 9c. Scatter for the 10 lowest nonzero modes is represented by R^2 estimators of linear least squares fit (R^2=1 representing exact similarity), these are presented in Table 2. The mode shapes also reveal that symmetric local plate deformation (Figure 4d) occurs between the stiffeners in the shell model, Figure 9b. This deformation is absent in ESL model result, Figure 9a. The present method accounts this deformation by analytic formulae and frequency iteration. The formulae are assuming local deformation by Eq. (18), this is compared with shell model results in Figure 9d for mode 5 at nodes highlighted in Figure 9b. Modes 11–23 of the shell model are local antisymmetric plate modes, and mode 24 of shell model is similar to 11th mode of the ESL model. This is due to ESL elements averaged bending stiffness, unable to find local plate modes compared to discrete stiffening of the shell model.

Mesh sensitivity for ESL models is performed by creating seven additional models (A to G). For these the number of elements between transversal T-beams are 2, 3, 4, 6, 8, 12, and 16 respectively, see Table 3. Consistent mass matrix (COUPMASS in NXNastran) is used in these analyses, as it is more accurate option for coarse meshes. The resulting natural frequencies are plotted in Figure 10, which illustrates the effects of mesh size, and length-scale interaction. Differences between models can be seen to increase with frequency. If 2.5% accuracy (in comparison to Model V) is considered sufficient, even coarsest Model A gives valid results up to mode 5, Model B up to mode 8, and Model C up to mode 10. If 1% accuracy is required, Model D is good enough for all 10 modes. Model E reduces the difference to less than 0.5%. Differences in frequencies between the finest models F, G, and V are very small.

Computational performance is studied by running (SOL 103) of NX Nastran 11.0.2® FE solver in a laptop computer with 32 GB of RAM by utilizing single core of Intel® Core™ i7-8850H processor. Numbers of modes found and the solution times are compared by applying 3 different output frequency ranges: 0–20 Hz, 0–30 Hz, and 0–40 Hz. The results are listed in Table 4. For the ESL models, number of modes found increases with DOFs. The models find 6–7 modes below 20 Hz, 19–24 modes below 30 Hz, and 29–52 Modes below 40 Hz. The shell model differs significantly, as it finds 10 modes below 20 Hz, 160 modes below 30 Hz, and 293 modes below 40 Hz. Most of these are antisymmetric local plate modes.

The solver times listed in Table 4 are real solver times in seconds taken from log files created by the solver software. The study is made for the validation structure, which is rather small. General conclusions should not be made about calculation times in very large thin-walled structures, as they could be more than 1000 times larger by volume (and by degrees of freedom). Relative differences in solver times appear rather small between the coarsest models, which may be caused by small size of the models. Some remarks, however, can be made by comparing solver times of ESL and shell model. There is clear difference between the Model V and Shell even if they share exact same number of DOFs. Model V is solved in 62%, 40%, and 39% of the time needed for the shell model for 0–20 Hz, 0–30 Hz, and 0–40 Hz, respectively. For model E, which gives very similar accuracy for the 10 lowest modes, the respective times are 7.7%, 4.3% and 3.3%.

4. Conclusions

Presented method enables usage of homogenized equivalent single layer (ESL) elements in FEM calculation model without sacrificing accuracy by re-introducing inertia-induced length-scale interaction of symmetric local waveforms by energy-based analytical equations. Implementation of the ESL elements allow more freedom in FE meshing, as the element boundaries do not need to follow secondary stiffener locations. In comparison with full 3D shell mesh, similar accuracy can be achieved with approximately 1/20 of the computational time for the case study structure. Part of the computational benefit is achieved due to possibility of using coarser mesh in ESL, and other from the avoidance of the antisymmetric local plate modes, which are slowing the solution of the 3D shell mesh FEM. The antisymmetric local plate modes involve vibration in stiffened plates in such waveforms that interact very little with longer length-scales. Thus, these can be ignored in global consideration. If this local vibration within stiffened plates is of interest, it can be assessed by more appropriate methods such as [26, 27].

Inertia-induced length-scale interaction was added to the results outside of the FEM formulation. Benefit of this approach is that vibration modes of the FEM model can be solved as a simple eigenvalue problem, Eq. (17), for which efficient algorithms are widely available. Drawback is that the feedback from local inertia to global shape is lost, leading to slight error in global mode shapes in higher modes (see Figure 9c). In terms of natural frequency, however, the results are in very good agreement with the 3D shell validation model (see Table 2). Furthermore, if the local deformation would be included in FEM formulation, it would lead to natural frequency dependent mass and stiffness matrixes.

Local consideration of the stiffened plates was based on series of assumptions. Continuous periodic structure assumption was made for the stiffened panels, cylindrical bending assumption for periodic unit, and long flexural waves of the global motion were assumed. The case study

structure violated some of the assumptions: (P_5) total size was very small to be considered continuous, (P_3) next to its opening with free edge had locally aspect ratio 1.6, which is too low to justify cylindrical bending. Despite these local violations of the assumptions the results were very good in terms of natural frequency. It thus seems that the present approach is robust against local small violations of the assumptions. This is important property considering practical applicability of the method. The studied first 10 modes of the structure had rather long flexural waves in all the panels so the long wave assumption was justified. Higher frequency modes, however, would have violated that assumption as well. Nevertheless, obtained range of the 10 precise modes is reaching above 20 Hz, which is sufficient range for typical vibration comfort evaluations for example in ship design [11–13].

The study was limited to free harmonic vibration of linear system. Challenges for the iteration convergence might occur in proximity of the local resonance, possibly requiring different initial guesses for the iteration [24]. Furthermore, applying damping in local consideration would avoid the singularity. Assessing these issues is left for future work. Some aspects of the paper, such as definition of the complex structure by set theory notations, might be useful also in considerations of other limit states important in ship design, such as buckling and ultimate strength.

Funding

This work was funded by Meyer Turku Oy. The financial support is gratefully acknowledged.

References

[1] L. Rayleigh (John William Strutt), Theory of Sound, MacMillan and co., London, 1877.
[2] C. Lanczos, An iteration method for the solution of the eigenvalue problem of linear differential and integral operators, J. Res. Natl. Bur. Stan., vol. 45, no. 4, pp. 255–282, 1950. DOI: 10.6028/jres.045.026.
[3] M. Olson, and C. Hazell, Vibration studies on some integral rib-stiffened plates, J. Sound Vib., vol. 50, no. 1, pp. 43–61, 1977. DOI: 10.1016/0022-460X(77)90550-8.
[4] D. Hitchings (ed.), Finite Element Dynamics Primer, NAFEMS, Glasgow, 1992.
[5] J. Spence, E. Favini, and C. Page, "SSC-470 Finite element modeling methods: vibration analysis for ships," Ship Structure Committee, 2015.
[6] A. Zambon, L. Moro, and M. Biot, Vibration analysis of superyachts: Validation of the Holden Method and estimation of the structural damping, Mar. Struct., vol. 75, pp. 102802, 2021. DOI: 10.1016/j.marstruc.2020.102802.
[7] T. R. Lin, J. Pan, P. J. O'shea, and C. K. Mechefske, A study of vibration and vibration control of ship structures, Mar. Struct., vol. 22, no. 4, pp. 730–743, 2009. DOI: 10.1016/j.marstruc.2009.06.004.
[8] J. Raikunen, E. Avi, H. Remes, J. Romanoff, I. Lillemäe-Avi, and A. Niemelä, Optimisation of passenger ship structures in concept design stage, Sh. Offshore Struct., vol. 14, no. sup1, pp. 320–334, 2019. DOI: 10.1080/17445302.2019.1590947.
[9] E. Avi, Equivalent shell element for passenger ship structural design, Aalto University Doctoral Dissertations 133/2021 Unigrafia, Helsinki, 2021.
[10] DNV GL AS, "Finite element analysis, Class guideline DNVGL-CG-0127," 2015.
[11] M. Biot, and FDe Lorenzo, Criteria for Designing Noise and Vibration Comfort of Passengers on Board of Ships, in 21st Congreso Panamericano de Ingenieria Naval, Montevideo, Uruguay, 2009.
[12] F. Besnier, L. Jian, L. Murawski, and M. Weryk, Evaluation of main engine and propeller excitations of ship hull and superstructure vibration, Int. Shipbuild. Prog., vol. 55, pp. 3–27, 2008.
[13] E. Avi, A. Laakso, J. Romanoff, H. Remes, and I. Lillemäe-Avi, Coarse mesh finite element model for cruise ship global and local vibration analysis, Mar. Struct., vol. 79, pp. 103053, 2021. DOI: 10.1016/j.marstruc.2021.103053.
[14] A. Mobasher Amini, D. Dureisseix, P. Cartraud, and N. Buannic, A domain decomposition method for problems with structural heterogeneities on the interface: Application to a passenger ship, Comput. Methods Appl. Mech. Eng., vol. 198, no. 41–44, pp. 3452–3463, 2009. DOI: 10.1016/j.cma.2009.06.020.
[15] E. Carrera, A. Pagani, and M. Petrolo, Use of Lagrange multipliers to combine 1D variable kinematic finite elements, Comput. Struct., vol. 129, pp. 194–206, 2013. DOI: 10.1016/j.compstruc.2013.07.005.
[16] E. Carrera, et al., Global-local plug-in for high-fidelity composite stress analysis in Femap/NX Nastran, Mech. Adv. Mater. Struct., vol. 28, no. 11, pp. 1121–1127, 2021. DOI: 10.1080/15376494.2019.1655689.
[17] E. Carrera, A. Pagani, and M. Petrolo, Component-wise method applied to vibration of wing structures, J. Appl. Mech., vol. 80, no. 4, pp. 041012-1–041012-15, 2013. DOI: 10.1115/1.4007849.
[18] E. Carrera, A. Pagani, and R. Jamshed, Refined beam finite elements for static and dynamic analysis of hull structures, Comput. Struct., vol. 167, pp. 37–49, 2016. DOI: 10.1016/j.compstruc.2016.01.015.
[19] E. Carrera, and A. Pagani, Free vibration analysis of civil engineering structures by component-wise models, J. Sound Vib., vol. 333, no. 19, pp. 4597–4620, 2014. DOI: 10.1016/j.jsv.2014.04.063.
[20] T. Cavallo, E. Zappino, and E. Carrera, Component-wise vibration analysis of stiffened plates accounting for stiffener modes, CEAS Aeronaut. J., vol. 8, no. 2, pp. 385–412, 2017. DOI: 10.1007/s13272-017-0244-5.
[21] T. Cavallo, E. Zappino, and E. Carrera, Free-vibration analysis of space vehicle structures made by composite materials, Compos. Struct., vol. 183, pp. 53–62, 2018. DOI: 10.1016/j.compstruct.2017.01.010.
[22] E. Avi, I. Lillemäe, J. Romanoff, and A. Niemelä, Equivalent shell element for ship structural design, Sh. Offshore Struct., vol. 10, no. 3, pp. 239–255, 2015. vol DOI: 10.1080/17445302.2013.819689.
[23] A. Laakso, E. Avi, and J. Romanoff, Correction of local deformations in free vibration analysis of ship deck structures by equivalent single layer elements, Sh. Offshore Struct., vol. 14, no. sup1, pp. 135–147, 2019. no DOI: 10.1080/17445302.2018.1561173.
[24] A. Laakso, J. Romanoff, and H. Remes, Free flexural vibration of symmetric beams with inertia induced cross section deformations, Thin-Walled Struct., vol. 119, pp. 1–12, 2017. DOI: 10.1016/j.tws.2017.05.032.
[25] B. Feeny, and R. Kappagantu, On the physical interpretation of proper orthogonal modes in vibrations, J. Sound Vib., vol. 211, no. 4, pp. 607–616, 1998. DOI: 10.1006/jsvi.1997.1386.
[26] D. Mead, and S. Parthan, Free wave propagation in two-dimensional periodic plates, J. Sound Vib., vol. 64, no. 3, pp. 325–348, 1979. DOI: 10.1016/0022-460X(79)90581-9.
[27] D. Mead, Wave propagation in continuous periodic structures: Research contributions from Southampton, 1964–1995, J. Sound

Vib., vol. 190, no. 3, pp. 495–524, 1996. DOI: 10.1006/jsvi.1996.0076.
[28] S. Timoshenko, and S. Woinowsky-Krieger, Theory of Plates and Shells, McGraw-Hill, Singapore, 1959.
[29] A. Noor, W. Burton, and C. Bert, Computational models for sandwich panels and shells, Appl. Mech. Rev., vol. 49, no. 3, pp. 155–198, 1996. DOI: 10.1115/1.3101923.
[30] J. Reddy, Mechanics of Laminated Composite Plates and Shells—Theory and Analysis, 2nd ed., CRC Press, New York, 2003.
[31] E. Carrera, Historical review of zig-zag theories for multilayered plates and shells, Appl. Mech. Rev., vol. 56, no. 3, pp. 287–308, 2003. DOI: 10.1115/1.1557614.
[32] E. Carrera, and A. Ciuffreda, A unified formulation to assess theories of multilayered plates for various bending problems, Compos. Struct., vol. 69, no. 3, pp. 271–293, 2005. DOI: 10.1016/j.compstruct.2004.07.003.
[33] J. S. Archer, Consistent mass matrix for distributed mass systems, J. Struct. Div., vol. 89, no. 4, pp. 161–178, 1963. DOI: 10.1061/JSDEAG.0000939.
[34] R. Blevins, Formulas for Natural Frequency and Mode Shape, Krieger Publishing Company, Malabar, FL, 1979. (Re-issued 1995.)
[35] R. Parnes, Solid Mechanics in Engineering, Wiley, Chichester, 2001.

Appendix A. Equivalent single layer element for stiffened plates

According to Ref. [22], a stiffened panel can be modeled with homogenized three-layered laminate element, where plate layer thickness equals t_p, web and flange layer thickness h_w and h_f correspond to the height of the stiffener web and flange, respectively. To model the stiffness couplings between stiffened plate and T-girders in realistic way, the reference plane of the laminate element is offset to top of the plate as it is shown in Figure A1. The element relationship between homogenized internal forces, strain and curvatures can be presented as

$$\begin{Bmatrix} \{N\} \\ \{M\} \\ \{Q\} \end{Bmatrix} = \begin{bmatrix} [A] & [B] & [0] \\ [B] & [D] & [0] \\ [0] & [0] & [D_Q] \end{bmatrix} \begin{Bmatrix} \{\varepsilon\} \\ \{\kappa\} \\ \{\gamma\} \end{Bmatrix}, \tag{A1}$$

where {N} is normal force, {M} moment and {Q} shear force vectors, which are related to strain $\{\varepsilon\}$, curvature $\{\kappa\}$ and out-of-plane shear strain $\{\gamma\}$ vectors by multiplying with stiffness matrices. Membrane [A], membrane-bending [B], and bending [D] stiffness matrices are obtained from following relations:

$$[A] = \int_{-tp}^{0} [E]_p dz + \int_{0}^{hw} [E]_w dz + \int_{hw}^{hw+hf} [E]_f dz, \tag{A2}$$

$$[B] = \int_{-tp}^{0} [E]_p z dz + \int_{0}^{hw} [E]_w z dz + \int_{hw}^{hw+hf} [E]_f z dz, \tag{A3}$$

$$[D] = \int_{-tp}^{0} [E]_p z^2 dz + \int_{0}^{hw} [E]_w z^2 dz + \int_{hw}^{hw+hf} [E]_f z^2 dz, \tag{A4}$$

where the plate layer elasticity matrix $[E]_p$ is described as a 2 D isotropic material. The web and flange layers have stiffness in two directions and are described using 2 D orthotropic material. The elasticity matrixes $[E]_w$ and $[E]_f$ are found by applying the Rule of Mixtures:

$$[E]_w = \frac{t_w}{S}\begin{bmatrix} E & 0 & 0 \\ 0 & 0 & 0 \\ 0 & 0 & 0 \end{bmatrix}, \quad [E]_f = \frac{b_f}{S}\begin{bmatrix} E & 0 & 0 \\ 0 & 0 & 0 \\ 0 & 0 & 0 \end{bmatrix}, \tag{A5}$$

where S is stiffener spacing. $[D_Q]$ is out-of-plane shear stiffness matrix, which includes the shear stiffness in stiffener direction D_{Qx} and transverse to stiffener direction D_{Qy}:

$$[D_Q] = \begin{bmatrix} D_{Qx} & 0 \\ 0 & D_{Qy} \end{bmatrix}, \quad D_{Qx} = k_{xz}(G_p t_p + G_w h_w + G_f h_f), \quad D_{Qy} = k_{yz}(G_p t_p), \tag{A6}$$

where G_p is the shear modulus for the plate layer. G_w and G_f are the shear moduli for web and flange layers, respectively and are obtained from using the rule of mixtures, similarly as it was done in Eq. (A5). k_{xz} is the shear correction factor in the xz-plane, which relates the stiffener maximum shear stress to the average shear stress, that is $k_{xz} = (\tau_{xz})_{avg}/(\tau_{xz})_{max}$. The shear correction factor k_{yz} follows Reissner-Mindlin plate theory and is taken as 5/6.

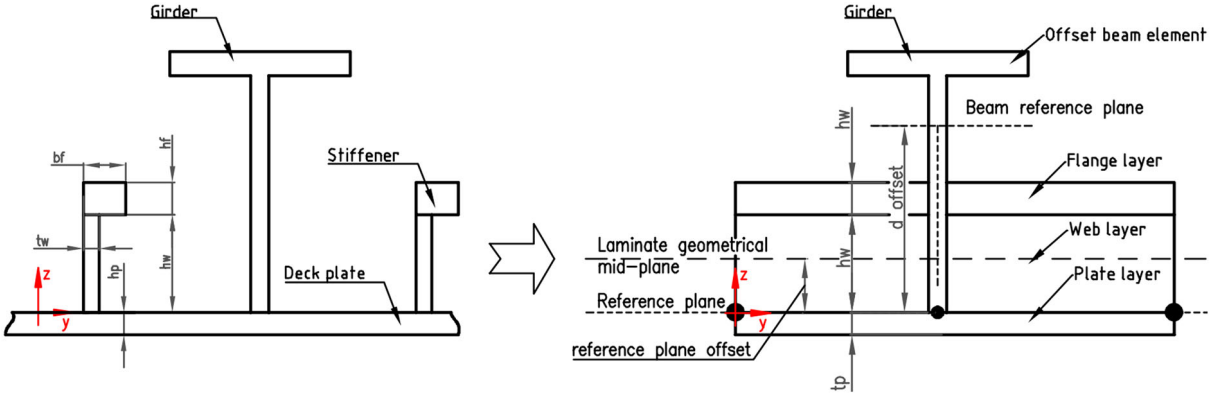

Figure A1. Stiffened panel division into three-layer laminate element and offset beam element [23].